Volume Title
ASP Conference Series, Vol. **Volume Number**
Author

ACCESS: Design, Calibration Strategy and Status

Kaiser, M. E.[1] and The ACCESS Team
, [1]*Johns Hopkins University, 3400 North Charles Street, Baltimore MD 21218*

Abstract. ACCESS, Absolute Color Calibration Experiment for Standard Stars, is a series of rocket-borne sub-orbital missions and ground-based experiments designed to enable improvements in the precision of the astrophysical flux scale through the transfer of absolute laboratory detector standards from the National Institute of Standards and Technology (NIST) to a network of stellar standards with a calibration accuracy of 1% and a spectral resolving power of 500 across the $0.35 - 1.7\mu$m bandpass.

Establishing improved spectrophotometric standards is important for a broad range of missions and is relevant to many astrophysical problems. Systematic errors associated with problems such as dark energy now compete with the statistical errors and thus limit our ability to answer fundamental questions in astrophysics.

1. Motivation

As a probe of the expansion history of the universe, using SNe Ia to distinguish dark energy models from one another levies a requirement for 1% precision in the cross-color calibration of the SNe Ia flux across a bandpass extending from $0.35 - 1.7\,\mu$m. However the systematic errors in the flux calibration network spanning the visible through the NIR currently exceed 1%. The astrophysical flux scale is ultimately pinned to a single star, Vega (Hayes & Latham 1975; Hayes 1985) through ground based measurements of a fundamental standard, a melting point black body furnace (Oke & Schild 1970). Since that fundamental calibration in 1970, there have been significant technological advances in detectors, telescopes and instruments, and the precision of the fundamental laboratory standards used to calibrate these instruments. These technologies have not yet been transferred to the fundamental astrophysical flux scale across the visible to NIR bandpass. In addition, Vega, the ultimate fundamental stellar standard for the astrophysical flux scale, has proven to be a poor choice for the following reasons. Vega is a pole-on rotator (Hill et al. 2010a; Yoon et al. 2008; Aufdenberg et al. 2006). As a result, it presents a range of effective temperatures and is difficult to model uniquely. It exhibits an infrared excess that arises from its circumstellar debris disk. And, it is too bright to be observed with today's premier optical telescopes.

This paper will describe the ACCESS program's strategy to obtain a set of precise ($< 1\%$) absolute flux measurements spanning the visible into the NIR for a set of stellar flux standards through observations from a rocket-borne telescope with a calibration tied to National Institute of Standards and Technology (NIST) fundamental irradiance (detector) standards.

2. ACCESS Overview

ACCESS - "Absolute Color Calibration Experiment for Standard Stars", is a series of rocket-borne sub-orbital missions and ground-based experiments that will enable the absolute flux for a limited set of primary standard stars to be established using calibrated detectors as the fundamental metrology reference (Kaiser et al. 2010b, 2008). These experiments are designed to obtain an absolute spectrophotometric calibration accuracy of $< 1\%$ in the $0.35 - 1.7\,\mu$m bandpass at a spectral resolution greater than 500 by directly tracing the observed stellar fluxes to NIST irradiance standards. Transfer of the NIST detector standards to our target stars will produce an absolute calibration of these standards in physical units, including the historic absolute standard Vega, the Sloan Digital Sky Survey (SDSS) standard BD+17°4708 (Fukugita et al. 1996), and the Spitzer IRAC standard HD 37725 (Reach et al. 2005).

3. Observing Strategy

ACCESS has adopted a multi-faceted strategy for reducing systematic errors and establishing the first members in a network of standard stars calibrated to 1% precision.

First in this multi-pronged approach is the elimination of the Earth's atmosphere as a spectral contaminant. One of the prime impediments to obtaining a precise flux calibration in the NIR is the plethora of hydroxyl (OH) lines that are formed high (~70 km - ~89 km) in the Earth's atmosphere (Moreels et al. 1977). These spectral lines are strong, numerous - extending across $0.85\,\mu\text{m} < \lambda < 2.25\,\mu$m, and highly variable on short timescales. Correcting ground based observations to 1 % precision for absorption by the Earth's atmosphere in the NIR is prohibitive. Spectral contamination by OH emission remains daunting even at balloon altitudes.

As a result, the ACCESS observations will execute from a sounding rocket platform completely above the Earth's atmosphere. The typical launch trajectory for a Black Brant IX sounding rocket carrying a 1000 lb payload yields an apogee of 300 km with the time above 100 km in excess of 400 seconds. Observing at an altitude exceeding 100 km eliminates the challenging problem of measuring the residual atmospheric absorption and strong atmospheric emission seen by ground-based observations and even by observations conducted at balloon altitudes. The number, strength, and variability of the OH lines was an important factor in the selection of a sounding rocket platform for the ACCESS observations.

Potential ACCESS stellar flux standards were selected based upon their ability to serve as precise calibration standards in both the visible and the NIR spectral region. This required that they (1) have existing photometric heritage, (2) present a stellar atmosphere capable of being precisely modelled, and are (3) bright enough to obtain a spectrum with S/N of 200 in a single rocket flight. Since our program includes observations of Sirius and Vega, which are 12hr apart on the sky, this also imposed the requirement that (4) additional targets be within 45° of the zenith on either the Sirius or Vega flight. To optimally utilize the flight time and to eliminate a step in the calibration transfer to larger telescopes, we required that (5) all targets other than Vega and Sirius be fainter than 6th magitude. The current set of ACCESS targets is presented in Table 1.

Further reduction of systematic errors will be achieved using a spectrograph with sensitivity extending from the visible through the NIR to eliminate this cross-calibration.

Key to achieving this broad bandpass is the use of WFC3 heritage HgCdTe detector whose sensitivity extends from below 4000 Å to $\sim 1.7\mu$m.

Another component of the calibration strategy is to establish an a priori error budget and track it.

Multiple methods will be used to determine the payload sensitivity through NIST traceable sub-system and end-to-end payload calibrations. A fundamental component of the calibration strategy is the use of NIST calibrated photodiode detector (irradiance) standards to establish NIST traceability. The NIST traceable photodiode irradiance standards will be used to establish the artificial star used to calibrate the integrated telescope and spectrograph. In addition to both an absolute and relative calibration of the payload, and hence the stars, the irradiance standards will establish the calibration system in fundamental physical units. End-to-end payload calibrations will be performed with both NIST continuum and emission line radiance standards as cross-checks for systematic errors.

ACCESS includes an On-board Calibration Monitor (OCM) to track the payload performance in the field prior to launch and while parachuting to the ground post-observation. The OCM will be calibrated at the same time as the payload and re-calibrated and monitored between flights.

Target	Alt Name	R.A. (2000)	Dec (2000)	Sp. Type	Vmag	Hmag
HD 37725		05 41 54	+29 17 51	A3V	8.35	7.92
HD 48915	Sirius	06 45 09	−16 42 58	A1V	-1.47	-1.39
HD 84937		09 48 56	+13 44 46	sdF5	8.28	7.12
HD 165459		18 02 31	+58 37 38	A1V	6.86	6.63
HD 172167	Vega	18 36 56	+38 47 01	A0V	+0.03	-0.03
BD+17 4708		22 11 31	+18 5 33	sdF8	9.47	8.11

Table 1. ACCESS primary and secondary targets.

A S/N of 200 per spectral resolution element over the full spectral bandpass will be achieved for the brighter targets in the sample. 0^{th} V magnitude stars Sirius and Vega will require subsecond integration times using subarray readouts to avoid saturation of the detector. For the fainter targets (e.g., BD+17°4708) a 400 second observation yields a S/N of 200 per spectral resolution element down to the Balmer edge. Additional binning can further increase the background subtracted signal-to-noise ratio of the acquired spectrum.

4. ACCESS Telescope and Spectrograph

The ACCESS telescope is a Dall-Kirkham cassegrain with a 15.6-inch diameter Zerodur primary mirror. The telescope mirrors have been coated with aluminum with a protective MgF_2 overcoat (section 6). This coating was chosen in order to retain sensitivity in the 3500−4000 Å range where the higher order Balmer lines provide leverage for stellar atmosphere modeling. The telescope feeds a low-order echelle spectrograph.

The spectrograph is a Rowland circle design configured as an echelle (Fig. 1) used in 1st (9000 – 19000 Å), 2nd (4500 – 9500 Å) and 3rd orders (3000 – 6333 Å), with some sensitivity in the 4th order. It consists of just two figured optical elements: a

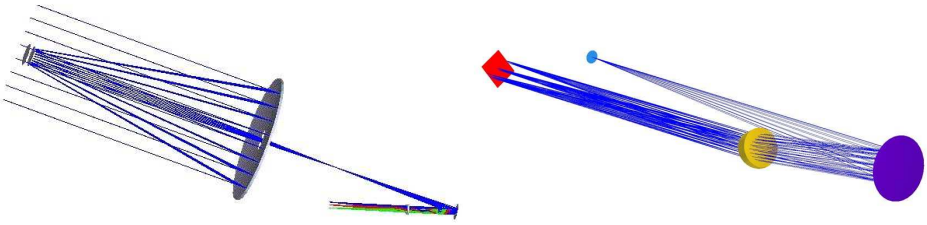

Figure 1. Left: Ray trace view of ACCESS. Parallel rays from the star enter the Dall-Kirkham Cassegrain telescope at left and are incident on the primary mirror (center of figure). The telescope secondary is at left in the figure and the grating is the optical surface at the extreme right.
Right: Ray trace view of the ACCESS spectrograph illustrating the grating on the right, the cross-dispersing prism, and the first three orders dispersed by the grating and incident on the detector at left.

concave diffraction grating with a low ruling density, and a Fery prism (Féry 1911) with spherically figured surfaces placed in the converging beam. The prism provides astigmatism correction and cross-disperses the spectrum.

The flight grating is a mechanically ruled (blazed), quad-partite, concave grating with a radius of curvature of 400.7 mm, a groove density of 45 lines per mm, and a groove depth of ~660 nm. The spectrograph design is optimized to use the grating through a range of small diffraction angles. This restricts the astigmatism generated by the Rowland circle mount configuration.

The prism is fabricated from LLF1 glass to provide high, relatively uniform, transmission and sufficient dispersion to separate orders and isolate the wings of the line spread function of adjacent orders on the detector across the bandpass extending from 3500 Å to 1.8 μm (Fig. 2).

The resolution of the spectrograph depends on the telescope point spread function (PSF) and the size of the detector pixels. For the telescope PSF of 1.17″ (as achieved on recent flights with a similar design) the 18 μm pixels of the detector provide critical sampling and produce constant wavelength resolution elements in each order, giving a resolving power ranging between 500 and 1000 (Fig. 2).

The spectrograph optical elements are sealed in a vacuum housing mounted to the back of the primary mirror base plate. An angled mirrored plate with a 1 mm aperture in the center located at the telescope focus serves as the slit jaw (McCandliss et al. 1994), allowing light to enter the spectrograph while reflecting the region surrounding the target into an image-intensified video camera for real-time viewing and control by the operator on the ground. A fused silica entrance window sits behind the slit jaw and provides the seal for the spectrograph vacuum housing. The grating and cross disperser are mounted inside along with a set of baffles. The detector is mounted on a bellows that is used as part of the focus adjustment mechanism.

5. Detector Performance

The focal plane detector array is a *HST*/WFC3 heritage HgCdTe device with a 1024×1024 pixel format and 18 μm×18 μm pixels. The detector composition is tailored to produce

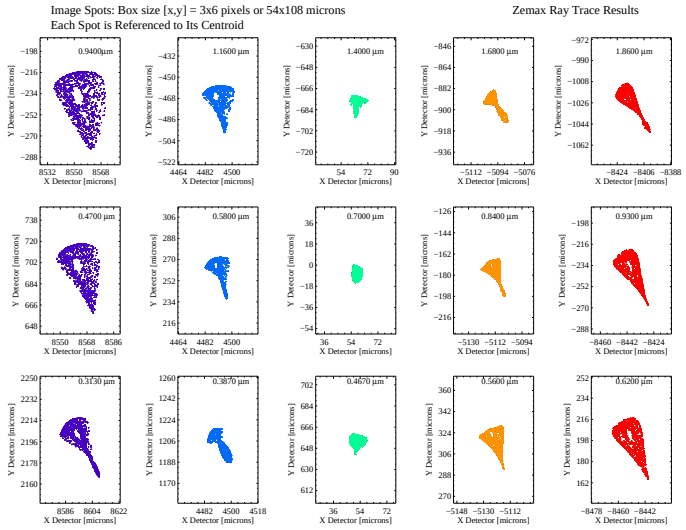

Figure 2. Spot diagrams for the optical layout at a selection of wavelengths spanning the ACCESS bandpass. Each box is labelled in microns and each spot is referenced to the chief ray. In general, the ray trace yields images that are within 2 pixels in the dispersion direction, ~4 pixels in the cross-dispersion direction.

a long-wavelength cutoff at $\sim 1.7\mu$ m. The CdZnTe growth substrate is removed to provide high near-IR quantum efficiency (QE) and response through the visible to 3500Å. The flight detector QE (Fig. 3) is ~ 30% at 5000Å. The band gap corresponding to the $1.7\,\mu$ m cutoff yields low dark current at operating temperatures near 140K (Fig. 3) and results in a detector that is relatively insensitive to thermal background radiation. A detector radiation shield, baffle, and cold stop will be cooled to ~200K to reduce the thermal background to an acceptable level. Cooling of the baffles is achieved through thermal inertia of a cold block that has been LN_2 cooled prior to launch. A Stirling cooler provides cooling for the detector.

The ACCESS detectors were selected based upon a suite of initial characterization tests conducted by GSFC in 2007 and the re-testing in 2011-2012 of key performance

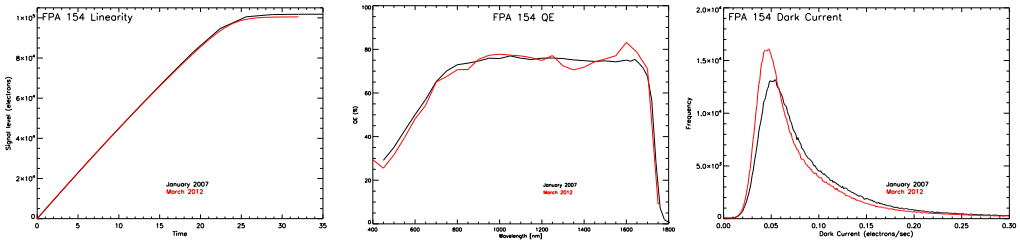

Figure 3. Left: Dectector linearity and full well capacity for FPA154 has not varied within measuerment error across the two epochs. Center: Quantum efficiency of FPA154. The QE data has been corrected for interpixel capacitance. Right: The dark current is ~0.05 electrons/sec for the pixel population and has not varied significantly. Data at each epoch were taken with the detector temperature at 145K.

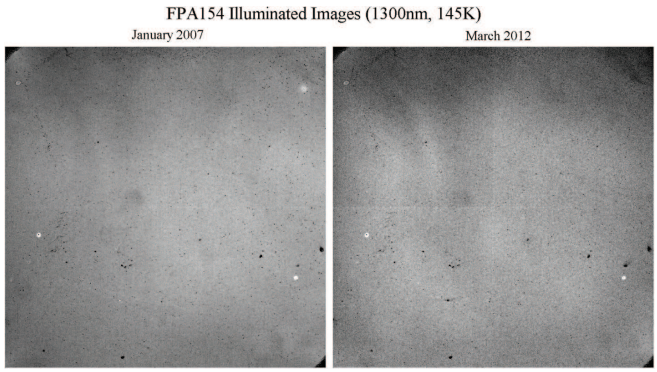

Figure 4. Flat field difference images taken at 1300nm as part of the test suite for assessing the detector qe, linearity, and full well performance. Lighter pixels have higher response.

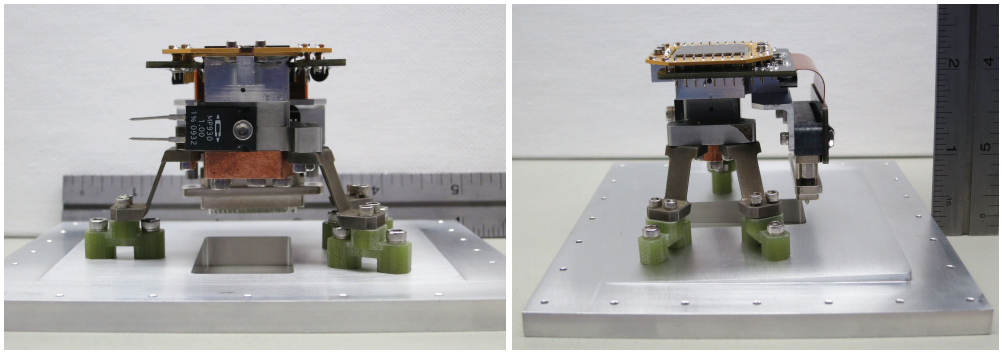

Figure 5. Left: Front view of detector with flight mount prior to vibration testing with launch loads. Right: Side view of detector with flight mount.

metrics such as dark current, read noise and quantum efficiecy and to extend the QE measurements to shorter (4000 Å) wavelengths. Reciprocity failure testing has been conducted to measure the count rate dependent non-linearity (Hill et al. 2010b).

FPA 154 and FPA 166 showed no significant performance changes over a ∼5 year baseline between measurements. Figure 3 illustrates the stability of the dark current, full well-linearity, and quantum efficiency performance metrics for FPA 154. At each epoch, illuminated flat field images at 1300 nm were acquired with diffent exposure times and were subtracted. A set of these difference images are shown in Figure 4.

6. Mirror Coatings

The primary and secondary telescope mirrors and the auto-collimating 18-inch flat mirror were coated with aluminum and a MgF_2 protective overcoat layer. Witness samples were used to determine (1) the reflectance as a function of the thickness of the MgF_2 and (2) to assess the spatial uniformity of the thickness of the MgF_2 layer across the

radius of the mirrors. Prior to coating the flight mirrors, witness samples were mounted along the radius, coated, and measured to determine the azimuthal and expected radial dependence of the reflectance (Figure 6). As expected, a slight radial dependence in the reflectance was found and modeled as a slight (50 Å) radial variation in the 275 Å thickness (expected from modeling of earlier coating tests) of the MgF_2 overcoat layer.

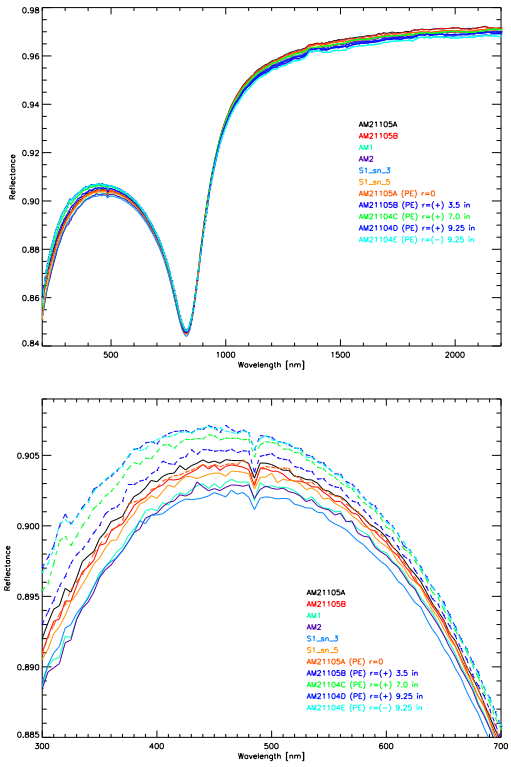

Figure 6. Top: Witness mirror reflectance measurements over the full ACCESS bandpass and extending to 2.2 μm. The solid lines indicate the reflectivity of the witness samples placed around the perimeter of the mirror during coating. The dashed lines indicate the predicted radial dependence of the reflectivity due the the radial dependence of the thickness of the MgF_2 overcoat. For each of the dashed curves, the radial position of the test mirror is presented in the legend. Bottom: Witness mirror reflectance measurements at wavelengths corresponding to the largest reflectance variation in the ACCESS bandpass. The solid lines and dashed lines are as described above.

The reflectance performance meets the ACCESS requirements. Spectrally, the radial spatial dependence is largest in the blue region of the ACCESS bandpass, with a maximum variation of ~0.4% occurring at 3500 Å to 3750 Å (dashed lines in Figure 6). The azimuthal and measurement variation was tracked by the witness mirrors located around the perimeter of the primary mirror. Again, the variation is largest in the blue spectral region, with a variation of 0.2−0.3% at 3750 Å to 4000 Å (solid lines in Figure 6). With the exception of the aluminum absorption feature near 8000 Å the reflectance exceeds 90% across the ACCESS spectral bandpass (3500 Å to 1.7 μm).

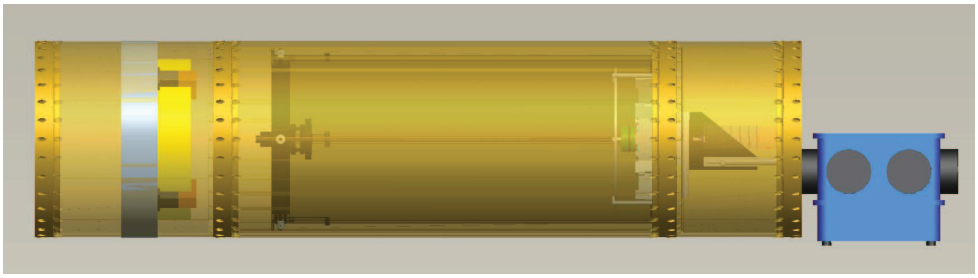

Figure 7. Auto-collimator subsystem used to calibrate the reflectivity of the collimator primary and secondary mirrors. From the right, a light source (not shown) feeds a vacuum monochromator, which is fiber fed into the auto-collimator housing to an order blocking filter and input to an integrating sphere. The output of the integrating sphere is baffled to match the collimator f-ratio. The light then passes through a pinhole at the focus of the collimator and is incident on the NIST standard photodiode detector which is positioned to measure the beam entering or exiting the auto-collimator. The auto-collimating flat mirror (yellow) is on the left. This assembly calibrates the collimator that will be feeding the artificial star-at-infinity to the telescope.

7. ACCESS Calibration

7.1. Calibration Overview

The crux of the ACCESS instrument sensitivity is knowing the ratio of the total number of photons entering the telescope aperture to the total number of photons detected by the spectrograph detector as a function of wavelength.

An artificial star will be used to provide a known source of photons for the telescope. The artificial star (Fig. 8 Right) consists of an illuminated pinhole placed at the collimator focus. The light illuminating the pinhole originates with a quartz tungsten halogen (QTH) continuum lamp fed to the vacuum monochromator. The output from the monochromater is fiber fed into the collimator vacuum housing. There it illuminates an order blocking filter, followed by an integrating sphere to generate a spatially uniform, unpolarized beam that is input to a baffle box to match the focal ratio of the stellar simulator beam to the F/12 collimator.

The total number of photons in the "star-at-infinity" output beam of the collimator will be provided by two measurements. The first is a measurement of the reflectivity of the auto-collimating flat mirror using a NIST calibrated photodiode detector standard. The second is a measurement of the intensity of the light from the stellar simulator that is input to and reflected by the auto-collimator. Figure 7 illustrates the auto-collimator calibration configuration used to determine the reflectivity of the primary and secondary mirrors. The absolute calibration transfer is obtained through the use of a NIST calibrated photodiode detector transfer standard to measure the input and output images at the auto-collimator focal plane.

The end-to-end calibration of the telescope with spectrograph (Fig. 8: Right) is then performed as a function of wavelength by measuring the intensity of the simulated star, measuring the count rate at the spectrograph detector, correcting for the collimator attenuation of the simulated star by the reflectivity of the collimator primary and sec-

ondary mirrors, and dividing the calibrated radiant flux by the illuminated area of the primary mirror.

Systematic effects, such as the uniformity of reflective coatings, matching of the collimator and telescope apertures, the spatial uniformity of the photodiode detectors, the transmission of the slit, the scattered light determination, the determination of the area of the primary and secondary telescope mirrors, the stability of the light source, etc., must be closely tracked if this process is to yield the required precision and accuracy.

In addition to the calibration of the ACCESS payload to a fundamental irradiance standard, ACCESS will be calibrated to both continuum and emission line fundamental radiance standards. Using emission from tunable lasers, the NIST SIRCUS facility (Brown et al. 2006a) will provide an end-to-end radiance calibration transfer to ACCESS while the use of a spectral light engine will calibrate ACCESS using a continuum spectral energy distribution similar to the spectral energy distribution of the stellar targets (Brown et al. 2006b).

7.2. Calibration Monitoring

An On-board Calibration Monitor (OCM) will track sensitivity changes in the telescope and spectrograph as a function of time before and after the absolute calibration data have been collected (Kaiser et al. 2010b, 2008; Kruk et al. 2008). The OCM citep-Kruk2008 uses 8 pairs of feedback stabilized LEDs, with central wavelengths spanning the ACCESS bandpass, to illuminate the telescope by scattering off a diffuser mounted on the interior of the telescope cover (Fig. 9). The LEDs are located in a multi-layer annular assembly mounted as a collar around the nose of the star tracker positioned behind the secondary mirror of the telescope. This assembly does not increase the central obscuration of the cassegrain telescope. Feedback stabilization is achieved through brightness monitoring of each LED by an adjacent dedicated photodiode. The OCM will monitor instrument performance during the end-to-end transfer of the NIST calibration of the diode standards to ACCESS in the laboratory. This light source will provide the capability to switch on-off during an observation to check the detector dependence on count rate.

8. Status

The ACCESS instrument and calibration hardware are in an active fabrication phase (Kaiser et al. 2010a). The telescope and collimator mirrors have been coated. The housing for the collimator and auto-collimating flat mirror systems have been fabricated. The collimator optics are ready for integration. The 18-inch flat mirror mount, rotary and translation stages have been fabricated, assembled, and control software written and testd. The flight detector has been selected and a subset of performance tests have been presented here. The detector mount assembly (Fig. 5) and housing have been vibration tested at launch levels and thermal acceptance testing has been performed at 130K. The first launch is expected within the year.

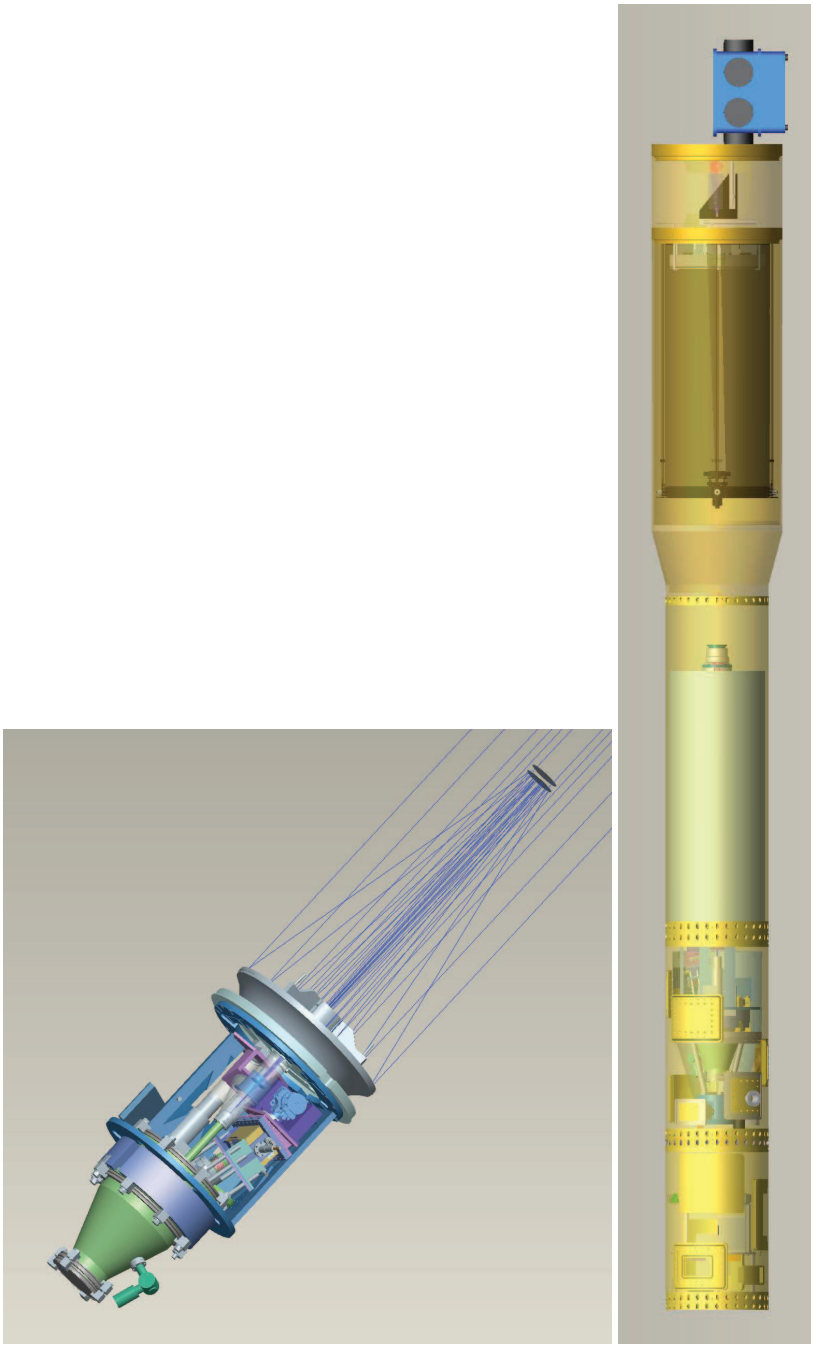

Figure 8. Left: The ACCESS telescope and spectrograph (not all components are shown). Right: Assembled ground calibration configuration of ACCESS with the collimated artificial star. From the top, a light source (not shown) feeds a monochromator, which is fiber fed to an order blocking filter and input to an integrating sphere. The output of the integrating sphere is baffled to match the collimator f-ratio. The light then passes through a pinhole at the focus of the collimator. This resulting collimated beam is the calibrated light source for the ACCESS instrument.

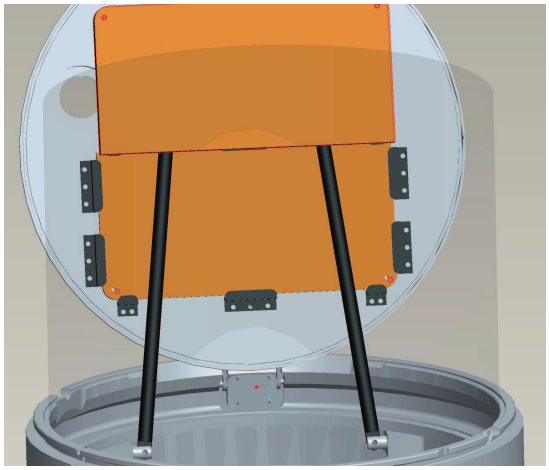

Figure 9. A spectralon diffuser is mounted on the inside of the telescope door. To maintain an unvignetted beam from the target star, the lower half of the diffuser is mounted under the arms that extend to open the aperture door during flight.

9. Summary

ACCESS is an active sub-orbital program with a payload development component followed by four launches over the subsequent two years. This experiment will enable a fundamental calibration of the spectral energy distribution of established bright primary standard stars, as well as standard stars 10 magnitudes fainter, in physical units though a direct comparison with NIST traceable irradiance (detector) standards. Each star will be observed on two separate rocket flights to verify repeatability to $< 1\%$, an essential element in establishing standards with 1% precision.

Acknowledgments. This research is being funded through NASA APRA-2007.

References

Aufdenberg, J. P., Mérand, A., Coudé du Foresto, V., Absil, O., Di Folco, E., Kervella, P., Ridgway, S. T., Berger, D. H., ten Brummelaar, T. A., McAlister, H. A., Sturmann, J., Sturmann, L., & Turner, N. H. 2006, ApJ, 645, 664. arXiv:astro-ph/0603327

Brown, S. W., Eppeldauer, G. P., & Lykke, K. R. 2006a, Appl.Optics, 45, 8218

Brown, S. W., Rice, J. P., Neira, J. E., C., J. B., & Jackson, J. D. 2006b, Appl.Optics, 111, 401

Féry, C. 1911, ApJ, 34, 79

Fukugita, M., Ichikawa, T., Gunn, J. E., Doi, M., Shimasaku, K., & Schneider, D. P. 1996, Ap. J., 111, 1748 (F96)

Hayes, D. S. 1985, in IAU Symp. 111: Calibration of Fundamental Stellar Quantities (Dordrecht: Reidel), 225

Hayes, D. S., & Latham, D. W. 1975, Ap. J., 197, 593

Hill, G., Gulliver, A. F., & Adelman, S. J. 2010a, ApJ, 712, 250

Hill, R. J., Malumuth, E. M., Foltz, R. D., Kimble, R. A., Waczynski, A., Boehm, N., Wen, Y., Kan, E., & Collins, N. R. 2010b, in Society of Photo-Optical Instrumentation Engineers (SPIE) Conference Series, vol. 7731, 115

Kaiser, M. E., Kruk, J. W., McCandliss, S. R., Rauscher, B. J., Kimble, R. A., Pelton, R. S., Sahnow, D. J., Dixon, W. V., Feldman, P. D., Gaither, B. W., Lazear, J. S., Moos,

H. W., Riess, A. G., Benford, D. J., Gardner, J. P., Hill, R. J., Kahle, D. M., Mott, D. B., Waczynski, A., Wen, Y., Woodgate, B. E., Bohlin, R. C., Deustua, S. E., Kurucz, R., Lampton, M., Perlmutter, S., & Wright, E. L. 2010a, in Society of Photo-Optical Instrumentation Engineers (SPIE) Conference Series, vol. 7731, 112

Kaiser, M. E., Kruk, J. W., McCandliss, S. R., Sahnow, D. J., Barkhouser, R. H., Van Dixon, W., Feldman, P. D., Moos, H. W., Orndorff, J., Pelton, R., Riess, A. G., Rauscher, B. J., Kimble, R. A., Benford, D. J., Gardner, J. P., Hill, R. J., Woodgate, B. E., Bohlin, R. C., Deustua, S. E., Kurucz, R., Lampton, M., Perlmutter, S., & Wright, E. L. 2010b, ArXiv e-prints http://adsabs.harvard.edu/abs/2010arXiv1001.3925K. 1001.3925

Kaiser, M. E., Kruk, J. W., McCandliss, S. R., Sahnow, D. J., Rauscher, B. J., Benford, D. J., Bohlin, R. C., Deustua, S. E., Dixon, W. V., Feldman, P. D., Gardner, J. P., Kimble, R. A., Kurucz, R., Lampton, M., Moos, H. W., Perlmutter, S., Riess, A. G., Woodgate, B. E., & Wright, E. L. 2008, in Society of Photo-Optical Instrumentation Engineers (SPIE) Conference Series, vol. 7014

Kruk, J. W., Kaiser, M. E., McCandliss, S. R., Orndorff, J., Barkhouser, R. H., Sahnow, D. J., Benford, D. J., Bohlin, R. C., Deustua, S. E., Dixon, W. V., Feldman, P. D., Gardner, J. P., Kimble, R. A., Kurucz, R., Lampton, M., Moos, H. W., Perlmutter, S., Rauscher, B. J., Riess, A. G., Woodgate, B. E., & Wright, E. L. 2008, in Society of Photo-Optical Instrumentation Engineers (SPIE) Conference Series, vol. 7014, 115

McCandliss, S. R., Martinez, M. E., Feldman, P. D., Pelton, R., Keski-Kuha, R. A., & Gum, J. S. 1994, in Society of Photo-Optical Instrumentation Engineers (SPIE) Conference Series, vol. 2011, 310

Moreels, G., Megie, G., Vallance Jones, A., & Gattinger, R. L. 1977, Journal of Atmospheric and Terrestrial Physics, 39, 551

Oke, J. B., & Schild, R. E. 1970, Ap. J., 161, 1015

Reach, W. T., Megeath, S. T., Cohen, M., Hora, J., Carey, S., Surace, J., Willner, S. P., Barmby, P., Wilson, G., Glaccum, W., Lowrance, P., Marengo, M., & Fazio, G. G. 2005, PASP, 117, 978. arXiv:astro-ph/0507139

Yoon, J., Peterson, D. M., Zagarello, R. J., Armstrong, J. T., & Pauls, T. 2008, ApJ, 681, 570. 0803.3145